Electronic Supplementary Information (ESI)

Pressure-induced hydrogen localization coupled to a semiconductor-insulator transition in a hydrogen-bonded molecular conductor

Akira Ueda,*[a‡] Kouki Kishimoto,[a] Takayuki Isono,[aǁ] Shota Yamada,[a,b] Hiromichi Kamo,[a] Kensuke Kobayashi,[c] Reiji Kumai,[c] Youichi Murakami,[c] Jun Gouchi,[a] Yoshiya Uwatoko,[a] Yutaka Nishio[b] and Hatsumi Mori*[a]

[a] *The Institute for Solid State Physics, The University of Tokyo, Kashiwa, Chiba 277-8581, Japan*

[b] *Department of Physics, Faculty of Science, Toho University, Funabashi, Chiba 274-8510, Japan*

[c] *Condensed Matter Research Center (CMRC) and Photon Factory, Institute of Materials Structure Science, High Energy Accelerator Research Organization (KEK), Tsukuba, Ibaraki 305-0801, Japan*

[‡] Present address: *Department of Chemistry, Kumamoto University, Chuo-ku, Kumamoto 860-8555, Japan*

[ǁ] Present address: *Department of Physics, Gakushuin University, Toshima, Tokyo 171-8588, Japan*

e-mail: aueda@kumamoto-u.ac.jp; hmori@issp.u-tokyo.ac.jp

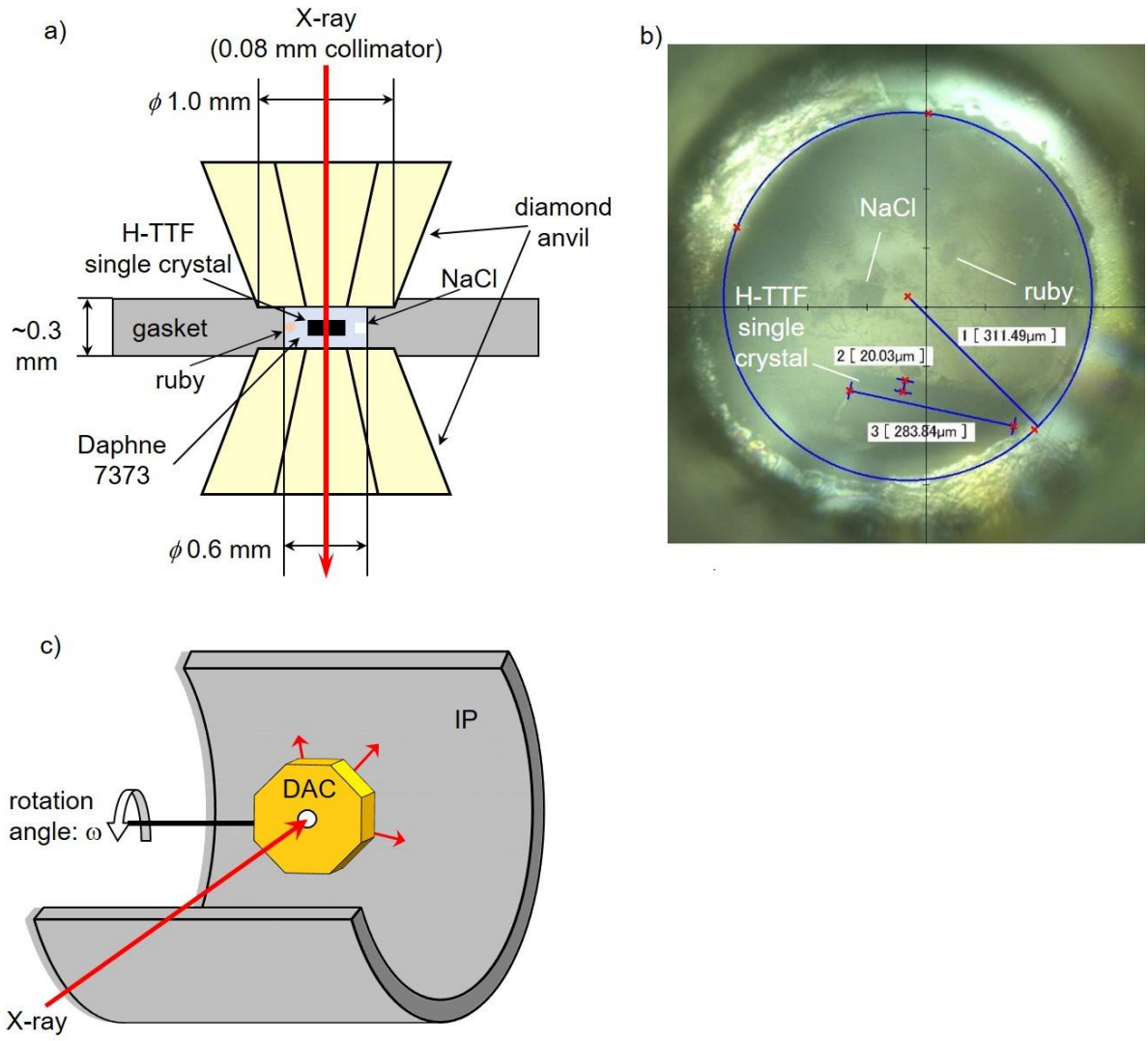

Fig. S1. Overview of the experimental setup for the synchrotron X-ray diffraction measurements on a H-TTF single crystal under hydrostatic pressure: (a) A schematic drawing of the diamond anvil cell (DAC) used in this study, (b) a photograph of the H-TTF single crystal, a NaCl single crystal (for pressure calibration at low temperatures), and a ruby chip (for pressure calibration at room temperature) in the DAC (filled with Daphne 7373 (the pressure medium)), and (c) a schematic drawing of the present X-ray diffraction measurements using the DAC.

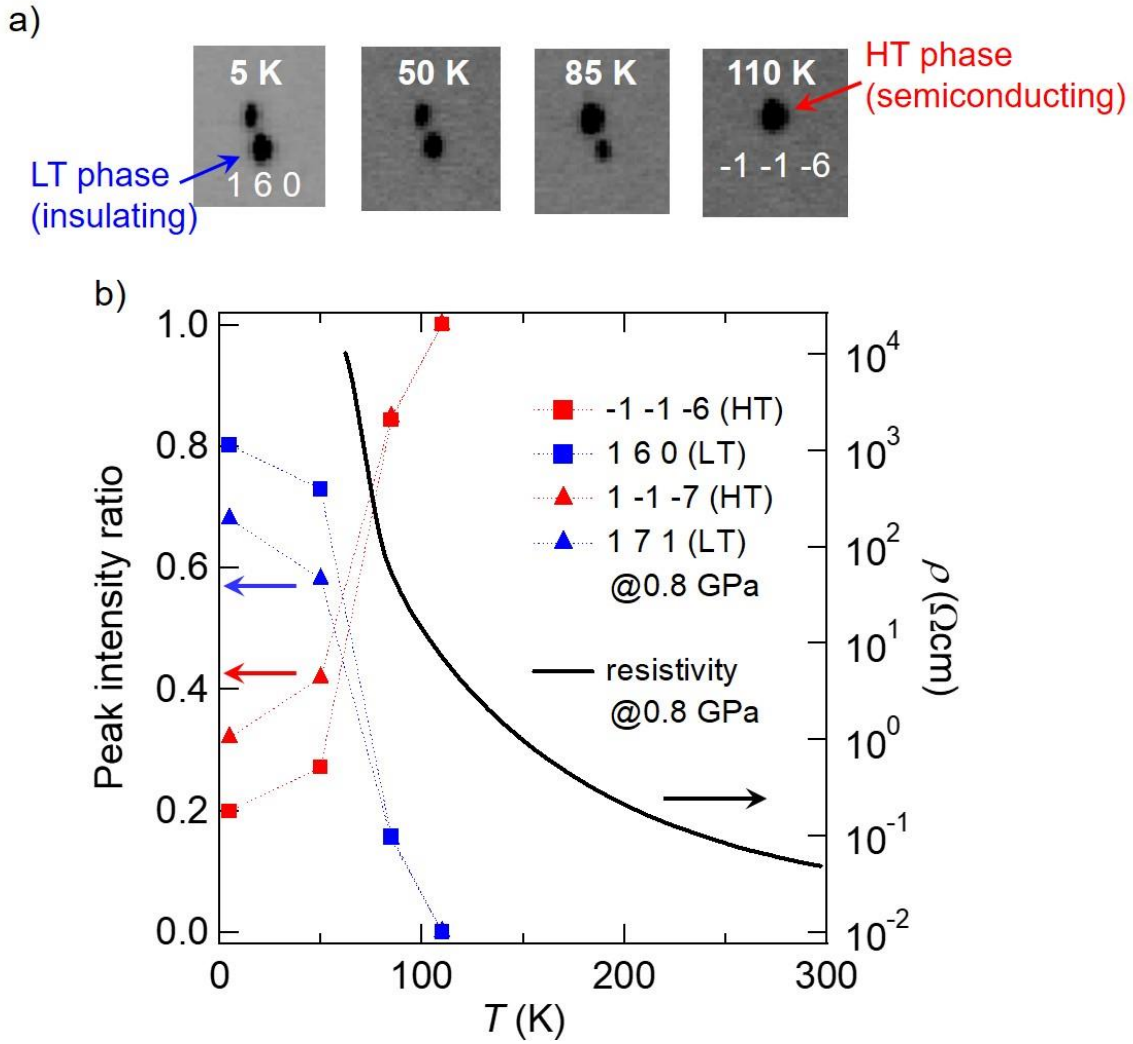

Fig. S2. X-ray diffraction measurements on a H-TTF single crystal at 0.8 GPa. a) Images of the diffraction spots of -1 -1 -6 in the high-temperature (HT) phase and 1 6 0 in the low-temperature (LT) phase measured at several temperatures and b) temperature dependence of the relative intensity ratios (left side) of two pairs of diffraction peaks in the HT (red symbols) and LT (blue symbols) phases. For comparison, the temperature dependence of electrical resistivity measured at 0.8 GPa is also shown in (b) (right side; identical to the data shown in Fig. 3a in text).

From the diffraction data, we have successfully determined the unit cell parameters of H-TTF in the LT (insulating charge-ordered) phase at 5 K at 0.8 GPa (Table 1 and S1) and in the HT (semiconducting dimer-Mott) phase at 293, 110, and 85 K at 0.8 GPa (Table S3).

Table S1. Unit cell parameters of the LT (insulating) phase of H-TTF at 0.8 GPa.

T (K)	5
Crystal system	triclinic
Space group	P-1 (#2)
a (Å)	8.220(7)
b (Å)	10.983(8)
c (Å)	14.982(11)
α (deg)	78.788(12)
β (deg)	78.46(3)
γ (deg)	89.575(18)
V (Å^3)	1299(2)

Table S2. Unit cell parameters of the LT (insulating) phase of H-TTF at 1.6 GPa.

T (K)	110	85	50
Crystal system	triclinic	triclinic	triclinic
Space group	P-1 (#2)	P-1 (#2)	P-1 (#2)
a (Å)	8.059(5)	8.049(5)	8.042(5)
b (Å)	10.788(6)	10.779(6)	10.779(5)
c (Å)	14.875(8)	14.867(8)	14.865(7)
α (deg)	78.710(10)	78.724(10)	78.717(9)
β (deg)	78.89(3)	78.96(3)	79.10(2)
γ (deg)	89.634(17)	89.723(17)	89.79(2)
V (Å^3)	1244(1)	1241(1)	1240(1)

Table S3. Unit cell parameters of the HT (semiconducting) phase of H-TTF at 0.8 GPa.

T (K)	293	110	85
Crystal system	monoclinic	monoclinic	monoclinic
Space group	$C2/c$ (#15)	$C2/c$ (#15)	$C2/c$ (#15)
a (Å)	29.34(2)	29.288(13)	29.267(12)
b (Å)	8.248(7)	8.183(4)	8.178(4)
c (Å)	11.082(9)	10.956(6)	10.944(5)
α (deg)	90	90	90
β (deg)	101.050(7)	101.217(4)	101.238(4)
γ (deg)	90	90	90
V (Å^3)	2632(4)	2576(2)	2569(2)

Table S4. Unit cell parameters of the HT (semiconducting) phase of H-TTF at 1.6 GPa.

T (K)	160	135
Crystal system	monoclinic	monoclinic
Space group	$C2/c$ (#15)	$C2/c$ (#15)
a (Å)	29.281(12)	29.207(13)
b (Å)	8.080(4)	8.065(4)
c (Å)	10.790(5)	10.776(5)
α (deg)	90	90
β (deg)	101.413(5)	101.402(4)
γ (deg)	90	90
V (Å^3)	2502(2)	2488(2)

Table S5. Crystallographic data for H-TTF at ambient pressure (1 atm, semiconducting phase).

T (K)	293[S1]	270	235	200
Formula	$C_{24}H_{15}O_4S_{12}$	$C_{24}H_{15}O_4S_{12}$	$C_{24}H_{15}O_4S_{12}$	$C_{24}H_{15}O_4S_{12}$
Fw	752.15	752.15	752.15	752.15
Crystal system	monoclinic	monoclinic	monoclinic	monoclinic
Space group	*C*2/*c* (#15)	*C*2/*c* (#15)	*C*2/*c* (#15)	*C*2/*c* (#15)
a (Å)	29.3300(5)	29.348(3)	29.35(2)	29.418(15)
b (Å)	8.4812(5)	8.4654(3)	8.450(6)	8.421(4)
c (Å)	11.2754(7)	11.2565(4)	11.225(9)	11.195(6)
α (deg)	90	90	90	90
β (deg)	100.8629(7)	100.911(6)	101.005(11)	100.912(7)
γ (deg)	90	90	90	90
V (Å^3)	2754.5(2)	2746.0(3)	2733(4)	2723(2)
Z	4	4	4	4
D_{calc} (g·cm^{-3})	1.813	1.819	1.828	1.834
λ (Å)	1.00000	1.00000	0.71073	0.71073
R_{int}	0.0119	0.0569	0.0686	0.0690
R_1 (I>2.00σ(I))	0.0345	0.0546	0.0705	0.0650
wR_2 (All reflections)	0.1220	0.1461	0.1880	0.1758
GOF	1.120	0.974	1.034	1.027
CCDC	894471	1896678	1896675	1896677

Table S5. (Continued) Crystallographic data for H-TTF at ambient pressure (1 atm, semiconducting phase).

T (K)	175	150	50[S1]
Formula	$C_{24}H_{15}O_4S_{12}$	$C_{24}H_{15}O_4S_{12}$	$C_{24}H_{15}O_4S_{12}$
Fw	752.15	752.15	752.15
Crystal system	monoclinic	monoclinic	monoclinic
Space group	*C*2/*c* (#15)	*C*2/*c* (#15)	*C*2/*c* (#15)
a (Å)	29.39(2)	29.44(4)	29.4273(8)
b (Å)	8.390(6)	8.383(12)	8.3637(2)
c (Å)	11.172(9)	11.176(17)	11.1334(7)
α (deg)	90	90	90
β (deg)	100.887(13)	101.55(2)	100.9180(9)
γ (deg)	90	90	90
V (Å^3)	2705(4)	2703(7)	2690.6(2)
Z	4	4	4
D_{calc} (g·cm^{-3})	1.847	1.848	1.857
λ (Å)	0.71073	0.71073	1.00000
R_{int}	0.0566	0.0831	0.0158
R_1 (I>2.00σ(I))	0.0619	0.0547	0.0326
wR_2 (All reflections)	0.1549	0.1397	0.0993
GOF	0.989	1.041	1.058
CCDC	1896676	1896674	894470

Table S6. Pressure dependence of the transfer integrals t_{b1}, t_{b2}, t_p, t_q (calculated by the extended Hückel method[S2]) and bandwidth W (obtained by the tight-binding method[S2]) in the HT (semiconducting) phase of H-TTF (see also Fig. S3 and S4 shown below).

Although the unit cell parameters of the HT phase under pressure were successfully determined in this study (Tables S3 and S4), the corresponding atomic coordinates were not determined. Therefore, we used the reported atomic coordinates (obtained at 1 atm at 293 K[S1]; see Table S5) for all the calculations and simply evaluated how the contraction of the unit cell (or the decrease in the intermolecular distances) affects the transfer integrals and bandwidth. The results (shown below) clearly demonstrate that these parameters are increased with increasing pressure, which should result in the decrease in the activation energy (E_a) in the HT semiconducting phase of H-TTF and D-TTF (Fig. 2 and 3 in text).

Pressure	1 atm (293 K)	0.8 GPa (293 K)	1.6 GPa (160 K)
t_{b1} (meV)	213	244	288
t_{b2} (meV)	79	94	108
t_p (meV)	41	47	58
t_q (meV)	–15	–16	–16
W (eV)	0.32	0.36	0.42

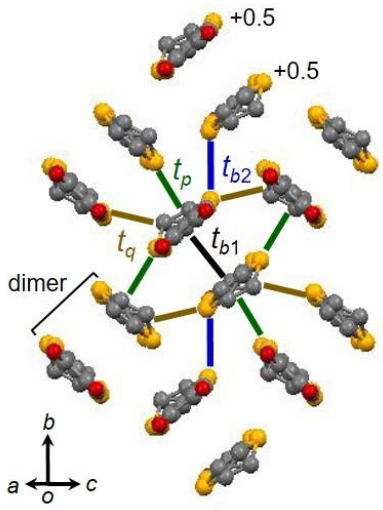

Fig. S3. Molecular arrangement and transfer integrals t_{b1}, t_{b2}, t_p, t_q in the HT (semiconducting) phase of H-TTF. The values of t_{b1}, t_{b2}, t_p, and t_q are summarized in Table S6.

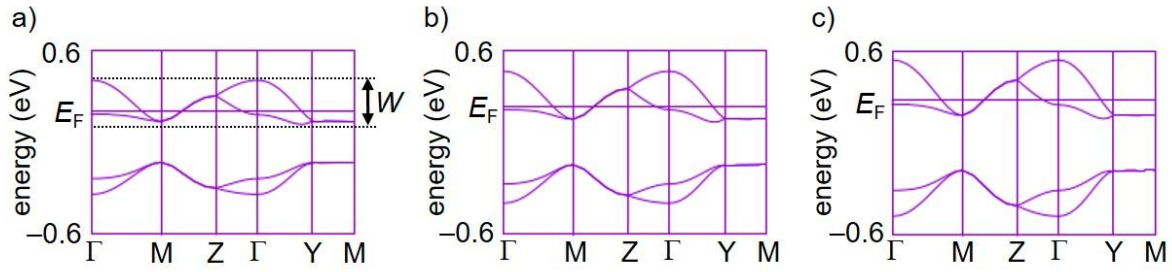

Fig. S4. Pressure dependence of the electronic band structure in the HT (semiconducting) phase of H-TTF: a) 1 atm (293 K), b) 0.8 GPa (293 K), and c) 1.6 GPa (160 K). The unit cell parameters used are those obtained at each condition (Tables S3–S5). The atomic coordinates used are those obtained at 1 atm (293 K).[S1] The values of the bandwidth W are summarized in Table S6, indicating an increase in W with increasing pressure.

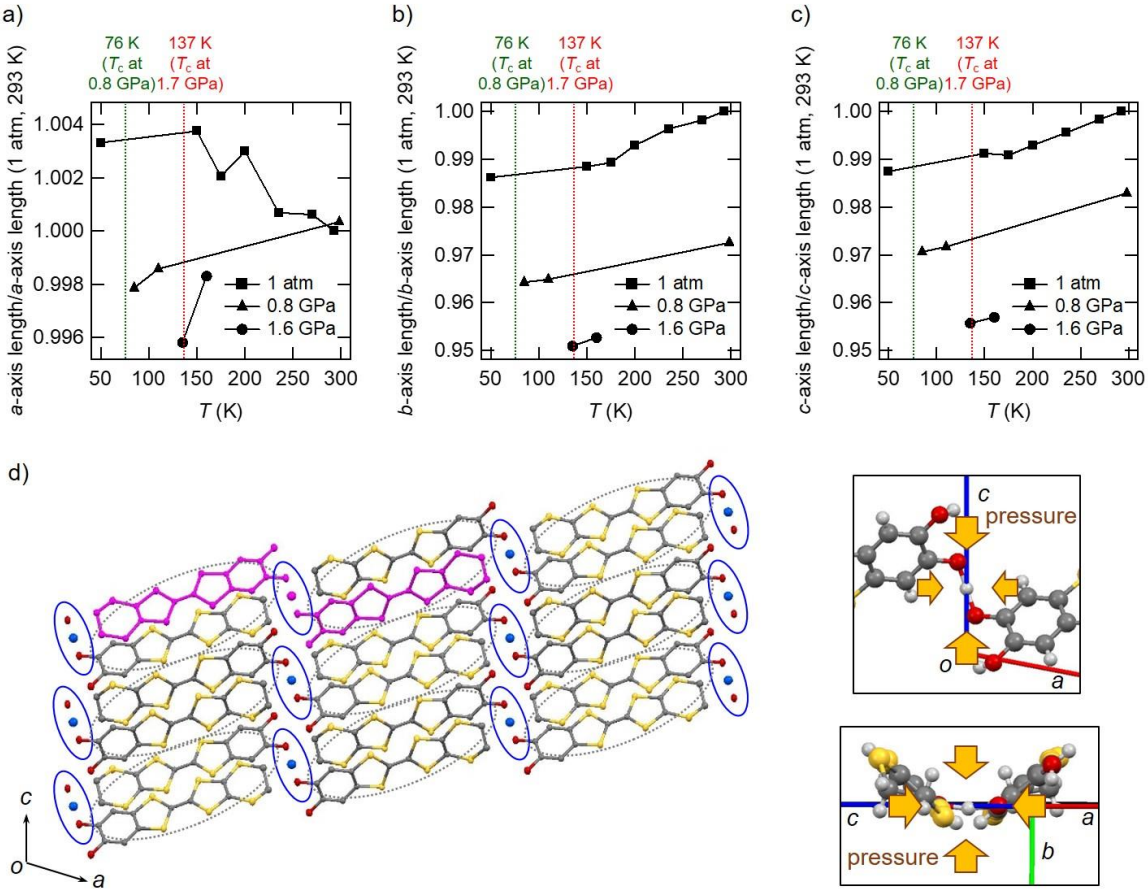

Fig. S5. Pressure- and temperature-dependent variations in the unit cell axis lengths of H-TTF in the HT (semiconducting) phase (a: *a*-axis, b: *b*-axis, and c: *c*-axis; normalized by the values at 1 atm at 293 K[S1]) (see also Tables S3–S5). d) A schematic illustration of the expected pressure effect on the hydrogen-bond moiety.

Here, the hydrogen bonds triggering the phase transition exist within the *ac*-plane (nearly along the *c*-axis), as shown in d). By applying hydrostatic pressure, the *c*-axis length is significantly decreased (c), which would lead to compression of the hydrogen bond (*i.e.*, the O···O distance). In addition, the *b*-axis, vertical to the hydrogen bond, is also significantly contracted (b), and furthermore, the *a*-axis is slightly contracted (a). Therefore, one can imagine that the hydrogen bond is not simply contracted but deformed by applying the pressure, similar to the case reported by Endo *et al.*[S3]. As a result, the original single-well energy potential curve in H-TTF[S4] might be transformed into a double-well one, leading to the hydrogen localization at low temperatures (Fig. 3b) and the following charge disproportionation/ordering.

In addition, the significant decrease in the *b*- and *c*-axis lengths indicates that the intermolecular distances in the conducting layers (the *bc*-plane, Fig. 1 and S3) are significantly

decreased by pressure, which should result in the increase in the transfer integrals and bandwidth (Table S6, Fig. S3 and S4) and the decrease in the activation energy (Fig. 2 and 3 in text).

References

S1. T. Isono, H. Kamo, A. Ueda, K. Takahashi, A. Nakao, R. Kumai, H. Nakao, K. Kobayashi, Y. Murakami and H. Mori, *Nat. Commun.,* 2013, **4**, 1344.

S2. (a) T. Mori, A. Kobayashi, Y. Sasaki, H. Kobayashi, G. Saito and H. Inokuchi, *Bull. Chem. Soc. Jpn.*, 1984, **57**, 627; (b) T. Mori, Energy band calculation software package. See: http://www.op.titech.ac.jp/lab/mori/lib/program.html.

S3. S. Endo, T. Chino, S. Tsuboi and K. Koto, *Nature,* 1989, **340**, 452.

S4. K. Yamamoto, Y. Kanematsu, U. Nagashima, A. Ueda, H. Mori and M. Tachikawa, *Phys. Chem. Chem. Phys*., 2016, **18**, 29673.